Steel and Composite Structures, *Vol. 55, No. 3* (*2025*) *211-224*
https://doi.org/10.12989/scs.2025.55.3.211

The mechanical behavior of multidirectional finned circular hollow steel damper: Analytical and numerical approach

Ali Awaludin[a], Andika M. Emilidardi[b], Angga F. Setiawan* and Iman Satyarno[c]

Department of Civil and Envinromental Engineering, Universitas Gadjah Mada, Grafika Street 2, Sleman, Special Region of Yogyakarta, Republic of Indonesia

(Received September 18, 2024, Revised April 6, 2025, Accepted April 7, 2025)

Abstract. This study investigates the mechanical behavior of a multidirectional finned circular hollow steel damper (MFCHSD) under cyclic loading by using numerical and analytical approaches. We propose to vary the surrounding an even number of scraped curved fins, i.e., four, six, and eight pieces, to improve the performance of the slender circular hollow steel damper (CHSD). The analytical approach implemented the classic analysis of shear stress distribution of thin walls, whereas the numerical approach adopted the finite element method with continuum shell element. Important characteristics, such as shear yield stress distribution, shear coefficient, shear yield strength, elastic stiffness, post-yield stiffness, and maximum strength, were examined. These parameters are used to predict the maximum-to-yield strength ratio and the post-yield-to-elastic stiffness ratio, which the important for the design of MFCSHD. Results suggest that the presence of additional fins increases CHSD performance in the form of shear yield strength, maximum strength, and post-yield stability. In addition, the shear yield stress distribution of the CHSD web was achieved, exhibiting good agreement between the analytical and the numerical approaches. Finally, the shear yield strength of MFCSHD could be quantified using a novel formulation in accordance with the shear stress distribution analysis.

Keywords: cyclic loading; fins; post-yield stability; shear stress distribution; shear yield strength

1. Introduction

Various types of metallic-yielding dampers have undergone extensive development; they serve as additional devices for dissipating energy in building and bridge structural systems (Abebe *et al*. 2019, Najari Varzaneh and Hosseini 2019, Nuzzo *et al*. 2018, Ying *et al*. 2019). Previous studies (Tanaka and Sasaki 2000, Vargas and Bruneau 2007, Guo *et al*. 2020, Javanmardi *et al*. 2020, Wang *et al*. 2021, Nyabongo and Li 2024) have demonstrated the efficacy of incorporating metallic dampers in building structures, enhancing structural stiffness, strength, and energy dissipation while reducing the structural response and preventingo damage to the main structural elements during seismic excitation. Similarly, in the context of bridge structures, metallic yielding dampers have been used as stoppers or shear keys for the upper structure relative to the substructure (Mosalam *et al*. 2015, Han *et al*. 2017, Setiawan *et al*. 2017). These dampers contribute to the prevention of unseating of the superstructure and dissipating earthquake excitation energy.

In numerous studies, researchers have examined the implementation of metallic-yielding dampers for reinforcing the structure and enhancing energy dissipation in multicolumn bridge piers (Chen *et al*. 2006). Among the commonly used metallic yielding dampers is the shear panel damper (SPD), well-known for its early yielding occurrence.

SPD presents several advantages, including cost-effective steel components, simple fabrication, high energy dissipation, and economical materials; it outperforms other seismic devices. These SPDs are made up of a web that offers shear resistance parallel to the loading direction with sufficient ductility. At the same time, flanges mitigate premature buckling when under confinement. A myriad of studies has explored the behavior and seismic performance of SPD (Chen *et al*. 2006, Zhang *et al*. 2012, Zhang *et al*. 2015, Chaofeng *et al*. 2017). In achieving better stable post-yield stiffness, further development combined of shear and bending mechanisms of yielding damper have been proposed (Men *et al*. 2023, Yang *et al*. 2023). An alternative approach to SPD development involves incorporating circular hollow sections (CHS). A comprehensive study of the mechanical behavior of circular hollow steel damper (CHSD) was conducted by Abebe *et al*. (2019). Conceptually, CHSD has the same mechanism of work as SPD, where the shear-yield mechanism on the device is used to dissipate earthquake energy. The shear-yielding mechanism occurs on the two arching sides of the 90° sector that are parallel to the shear loading direction. The other two arching sides of the 90° sector, which are

*Corresponding author, Assistant Professor
E-mail: angga.fajar.s@ugm.ac.id
[a]Associate Professor
E-mail: ali.awaludin@ugm.ac.id
[b]Lecturer
E-mail: andika.emilidardi@ugm.ac.id
[c]Professor
E-mail: imansatyarno@ugm.ac.id

http://www.techno-press.com/journals/scs&subpage=8
ISSN: 1229-9367 (Print), 1598-6233 (Online)

(a) (b)

Fig. 1 Experimental test of CFSD by Abebe *et al*. (2019): (a) specimen deformed shape and (b) cyclic loading protocol

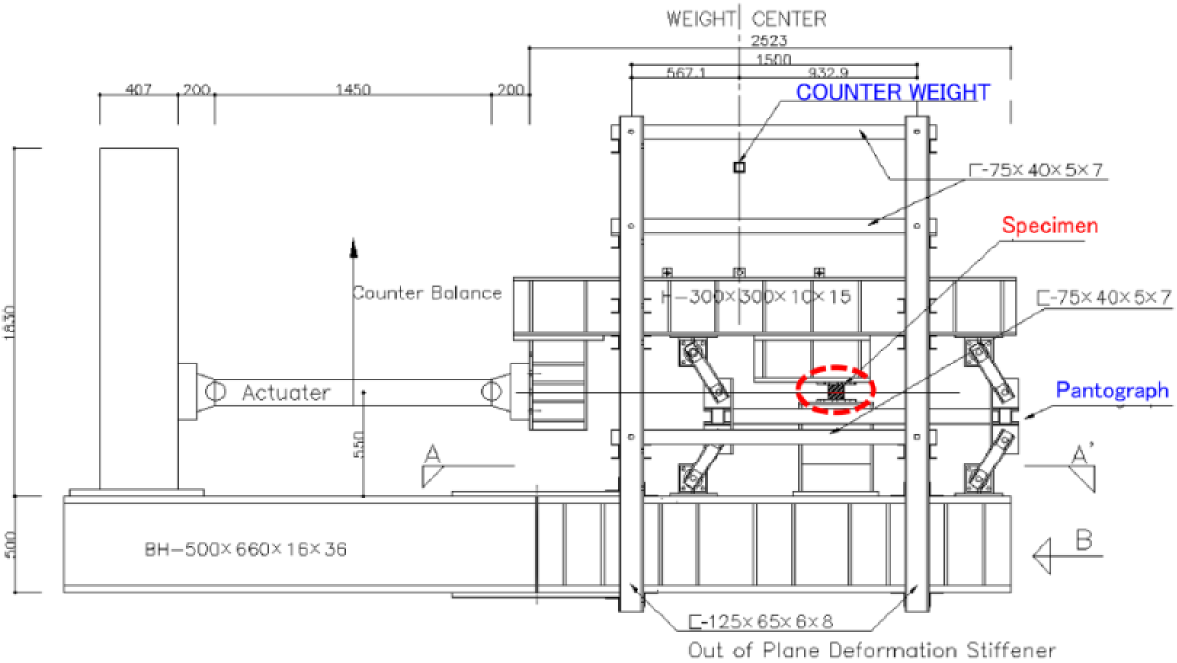

Fig. 2 The experimental test set up by Abebe *et al*. (2019)

perpendicular to the shear loading direction, function as flanges. Due to being categorized as radially symmetrical rotation sections, CHSD could be utilized as damper device work under a multidirectional loading parallel to the cross-section direction (Emilidardi *et al*. 2022). Thus, CHSD has the potential to be applied as a multidirectional damper in ordinary bridge structures, which have multidirectional relative movement between the superstructure to the pier.

According to Abebe *et al*. (2019), the limitations in the development of CHSD are mainly due to slenderness (D/t ratio). The results indicate that CHSD with D/t ratios exceeding 27.8 becomes slender and susceptible to premature buckling occurrence, thereby decreasing ultimate displacement, post-yield stiffness stability, and energy dissipation capacity. The challenge is that in the real steel materials market, the steel plates that are widely available with various mechanical specifications are thin in shape. Inspired by (Utomo *et al*. 2015, Emilidardi *et al*. 2021), the addition of fins to CHSD can overcome the premature buckling problem. In the study by Utomo *et al*. (2015), the two pieces of fins with curved shapes outer edges were added to a CHSD for premature buckling prevention under unidirectional shear loading. In another study results by Emilidardi *et al*. (2021), an additional event number of rectangular-shaped fins could prevent premature buckling but provoke stress concentration of the extreme cross-section fiber position of the fin. This concept adds complexity to the design phase of CHSD because it requires a complicated numerical approach using finite element methods to determine mechanical parameters on yielding and ultimate state (Utomo *et al*. 2015, Emilidardi *et al*. 2021). Detailed research on this aspect has not been conducted thus far. Therefore, an investigation is necessary to gain a better understanding of the characteristics and behavior of fined CHSD.

For the structural design application purposes of a new proposed structural element member, an experimental study could exhibit realistic results to confirm the proposed theoretical formulation (Feng *et al*. 2021a, Wang *et al*. 2021) , however, in achieving sufficient multi-parameters for design, it needs a huge number effort and resources. One simple and accurate method for reducing the amount of experimental testing numbers is developing a numerical model with a finite element method (FEM) by calibrating some models from the represented experimental studies (Feng *et al*. 2021b, Feng *et al*. 2021c, Wang *et al*. 2025).

Then, the calibrated FEM models were replicated for parametric study. Some studies conducted finite element analysis in investigating the mechanical behavior of steel structure element members from some experimental results of predecessor studies, i.e., Ghosh *et al*. (2025) investigated the axial capacity of cold-formed steel channels section with slit, Wang *et al*. (2024) modeled the cold-formed steel with circular web opening under two-flange loading to develop the strength with the direct method. However, the mentioned studies above about numerical modeling calibrated to the experimental and parametric study with FEM have not yet been implemented for CHSD devices.

The present study investigates the structural behavior of a multidirectional CHSD featuring a slender tubular section with fins, namely, a multidirectional finned circular hollow steel damper (MFCSHD). MFCHSD is engineered with a slender tubular from steel plate with the confinement of the surrounding fins. The MFCHSD is intended to be applied as a seismic energy dissipation device for simple support structural bridge systems. It aims to dissipate seismic excitation energy by facilitating arbitrary lateral relative displacement between the girder and the pier. The seismic properties of the proposed MFCHSD require a comprehensive study, including theoretical and experimental aspects, to facilitate its practical engineering applications. Numerical computations, particularly using the finite element method, are essential in this assessment. The preliminary investigation of the analytical and numerical simulations approach of seismic behavior associated with finned tubular MFCHSD was conducted following the predecessor study performed by Abebe *et al*. (2019). Several scenario variables with the addition of an even number of fins are arranged around the web to shorten the chord span of the tubular web in preventing premature buckling, as in the study by Emilidardi *et al*. (2021). The curved shape fins were adopted following Utomo *et al*. (2015) expected to reduce the stress concentration of the fins, which leads to tearing. Important features, such as shear yield stress distribution, shear coefficient, and backbone curve characteristics with parameters, i.e., shear yield strength, maximum shear strength, elastic stiffness, post-yield stiffness, and post-yield stability, were examined.

2. Analysis Method

2.1 Validation of CHSD model

The numerical model of CHSD was validated following the research of Abebe *et al*. (2019), who investigated the inelastic behavior of CHSD with different diameter-to-thickness ratios, D/t. Abebe *et al.* (2019) conducted experimental and numerical studies of CHSD with dimensions of 80 mm height, 48.6 mm inner diameter, and 2.5 mm thickness (D/t ratio 19.4), as shown in Eq. (1). In addition, numerical analysis of varied higher D/t ratios of the CHSD was conducted. The experimental setup is illustrated in Fig. 2, where the CHSD bottom support was fixed for translation and rotation, whereas the upper support allowed translation motion but was fixed against rotation.

The results suggest that the hysteresis loop of the numerical model (D/t ratio 19.4) agreed with the experimental results. Subsequently, Abebe *et al*. (2019) investigated the behavior of the tubular CHSD for higher values of D/t ratios.

In the present study, prior to adding the fin to the CHSD, a numerical model validation of CHSD is conducted in accordance with the research of Abebe *et al*. (2019). This investigation aims to determine appropriate modeling input parameters related to the hysteresis loop achievement as the baseline. Numerical model validation was conducted for the input parameters of the material model and CHSD model without fins (V0) for D/t ratios equal to 19.4 and 48.6. In the research of Abebe *et al*. (2019), the steel material used was SS400. Thus, in this study, the SS400 input material was verified by modeling a steel tensile test using finite element analysis. The input parameters of the material model considered the combination of isotropic and kinematic hardening, following the study of Chaboche (1986). The numerical analysis results of the steel tensile test model were in accordance with the experimental results from the research of Abebe *et al*. (2019), as shown in Fig. 3(a). In addition, numerical validation was carried out on the CHSD V0 model with D/t variations of 19.4 and 48.6. The results of the hysteresis graph in the numerical model of this study demonstrate a discrepancy in the form of no strength degradation at the end of maximum displacement. This occurrence can be attributed to the modeling assumption that does not consider ductile fracture. Nevertheless, the numerical analysis in the current study exhibited consistent results with the research conducted by Abebe *et al*. (2019), as shown in Fig. 3(b) and Fig. 4. Thus, the numerical model input parameters could be used for other varied specimen models with additional fins.

2.2 Proposal for seismic performance enhancement of CHSD with additional fins

In this study, the validated numerical model of the V0 CHSD with a D/t ratio of 48.6 was modified by adding fins, that is, four, six, and eight fins for each type, namely, V4, V6, and V8, respectively. Thus, the specimen model variations, i.e., CHSD and finned CHSD (MFCHSD) consisting of a web and fins, are shown in Figs. 5-6, respectively. The fin thickness is twice the thickness of the web, as described in Chen *et al*. (2006). The additional fins are proposed to enhance the confinement of the tubular web, preventing premature buckling and resulting in more stable post-yield stiffness. Based on the research of Emilidardi *et al*. (2022), stress concentration was identified at the connection area of the fins and baseplate in straight-shaped (rectangular) fins. This finding indicates that the connection area of the fins model has the potential to undergo tearing under large plastic deformation. In the study (Utomo and Antonius 2018) with a transition curve-shaped edge fins model, the stress concentration actually occurs on the curved side of the fins away from the connection area between the fins and the baseplate. Therefore, fin geometry was designed with a curved transition of the outer edge to transfer the stress

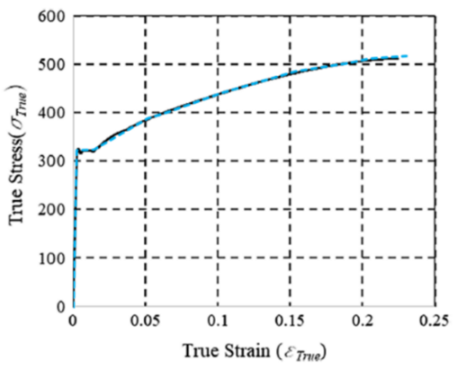

(a)

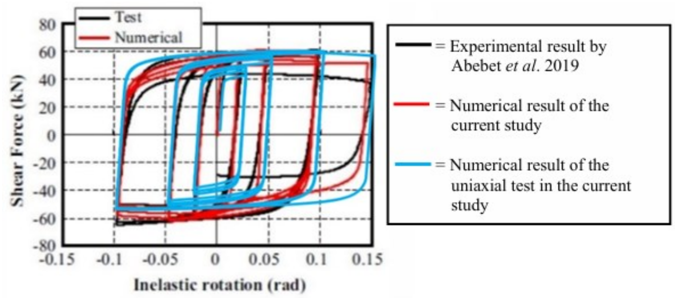

(b)

Fig. 3 Validation results: (a) uniaxial test for the SS400 material and (b) cyclic test of the MSPD V0 with a D/t ratio of 19

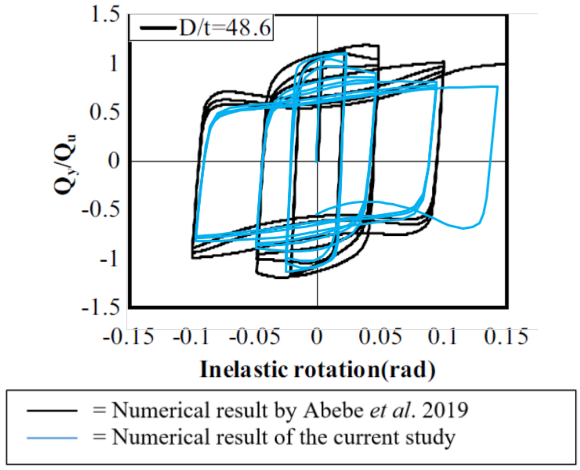

Fig. 4 Validation results of the cyclic test of the MSPD V0 with D/t ratio of 48.6

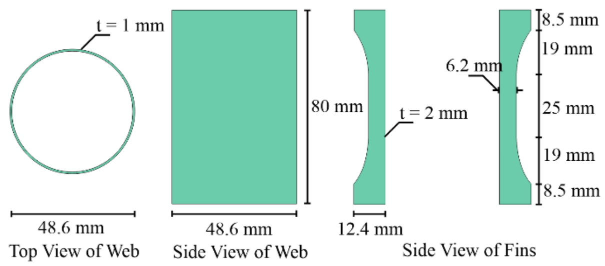

Fig. 5 Dimension and configuration of circular hollow steel damper and finned circular hollow steel damper

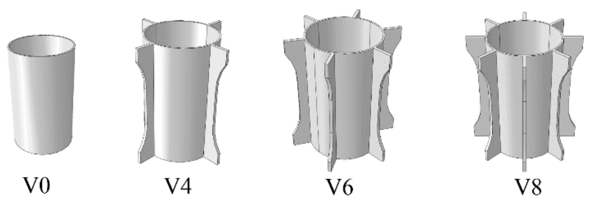

Fig. 6 Illustration of every variant of circular hollow steel damper and finned circular hollow steel damper.

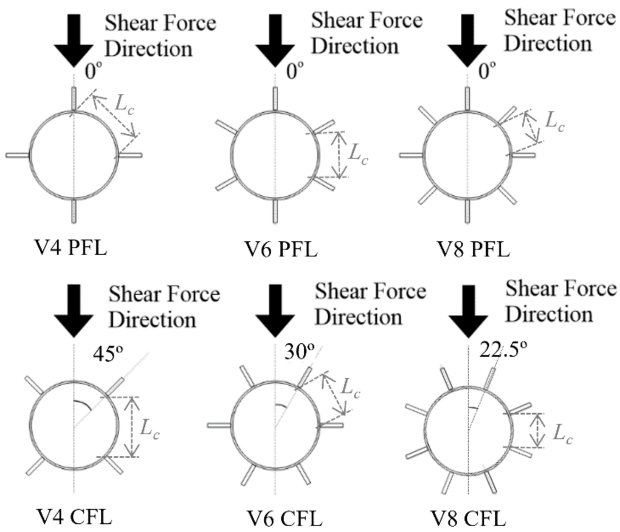

Fig. 7 CHSD and MFCHSD loading direction.

concentration from the side of the fin–base plate connection to the transition zone.

In this study, each type of CHSD and MFCHSD was subjected to the same loading protocol as the model proposed by Abebe *et al.* (2019). The loading direction was applied on the (parallel fins line) PFL and cross fins line (CFL) axis of each variation to investigate the shear resistance consistency.

The addition of an even number of fins (i.e., 4, 6, and 8) aims to achieve symmetrical geometry along both the PFL and CFL axes to achieve the most uniform shear resistance under multidirectional loads. Furthermore, the increased number of fins can shorten the chord length L_c expected to reduce the local slenderness (L_c/t) of the tubular web to prevent premature buckle occurrence, as shown in Fig 7. The approach begins with the smallest number of fins, ensuring the presence of both PFL and CFL axes. Choosing an even number of fins facilitates the identification of the probable weakest condition of CFL axis. The shear yield stress distribution in the web on the yielding state was studied for each CHSD and MFCHSD, ranging from type V0 to V8. The shear yield stress distribution of the tubular web is important information in investigating the correlation between the additional fins to the shear yield strength achievement according to the stress flow mechanism concept. Furthermore, the shear yield strength is an important parameter for the shear strength design in the developing backbone curve of the MFCHSD.

2.3 Shear yield stress distribution of the web

In revealing the presence of the fins to the shear yield stress distribution of the web, two methods are to be used: analytical and numerical. Analytical methods used classical shear stress distribution, as expressed in Eq. (1). The web section was divided into several strips, where each strip represents the shear stress value that occurs on the web side, to determine the shear stress value on each web side. The strip division method was divided on the most optimum strip thickness. It can be divided based on the outer diameter of the section. As illustrated in Fig. 8, the closer to the boundary, the strip will widen slightly. This calculation is in accordance with the reference (Bukkems 2017). Then, the shear stress results for each strip are plotted in a graph to determine the distribution of shear stress on the web, as shown in Fig. 9. The peak shear stress must be confirmed to reach the initial yielding state. The shear stress from the analytical method was oriented parallel to the load direction. The numerical method involved collecting the initial shear yield stress of the web in each mesh. Moreover, the shear yield stress was determined using the shear yield stress condition of the analytical results. The numerical shear yield stress orientation is still based on the local axis; it needs to be converted parallel to the load direction using Eq. (2), which includes shear stress (τ), local shear stress (τ_l), and mesh angle (θ).

$$\tau = \frac{VQ}{It} \tag{1}$$

$$\tau = \tau_l \, sin\theta \tag{2}$$

In evaluating the effect of the shear yield stress distribution of CHSD related to the shear yield strength achievement, the shear coefficient (k) value according to Timoshenko's beam theorem (Timoshenko 1921) is the basic concept. Then, the shear coefficient of some cross-section types was further developed by Cowper (1966) and Hutchinson (2001). In the case irregular section of finned circular hollow section (CHS), the shear coefficient is calculated according to the integration of the distributed shear stress (τ) and maximum shear stress (τ_{max}) on the web area (A) as formulated in Eq. (3). The shear coefficient could also represent the cross-section effectiveness of resisting shear force.

$$k = \int_A \frac{\tau}{\tau_{max}\, A} dA \tag{3}$$

2.4 Shear yield strength of the CHSD web

The shear strength in CHSD was calculated by integrating the shear stresses in the web and fins. According to Specification for Structural Steel Buildings (AISC 2016), the shear yield strength in a regular CHS is determined using Eq. (4), where f_y denotes the yield stress of steel, and A_g indicates the member's gross cross-sectional area. The shear yield strength divided by two indicates that the code used 0.5 for the shear coefficient value. The code uses the shear yield strength value 0.6 of the tensile yield strength (f_y). For the irregular CHS, i.e., surrounded by some fins, the shear yield strength of the circular hollow web is calculated by integration of shear stress following Eq. (5) by considering the initial shear stress (τ_i), final shear stress (τ_{i+1}) of each mesh area (dA_m). The web shear yield strength was obtained analytically for each variation of V4, V6, and V8 with considering PFL and CFL axes cases.

$$V_{yw} = \frac{0.6 f_y A_g}{2} \tag{4}$$

$$V = \int_{i=0}^{n} \frac{\tau_i + \tau_{i+1}}{2} \, dA_m \tag{5}$$

The occurrence of stress concentration in the tube of the web, fins, and web-fins connection boundary when subjected to service loads or minor earthquake occurrence can provoke fatigue phenomenon. In such cases, the proposed seismic device may be unable to dissipate designed earthquake energy properly due to premature failure from fatigue. Therefore, the stress concentration needs to be monitored. In monitoring the shear stress and axial stress concentration under the yielding state, we use the numerical analysis of the FEM model. The FEM model could consider axial and shear stress constellation adapting the geometrical configuration. While, the analytical approach could not capture stress concentration due to only considering shear stress distribution according to the Sant-Venant Equation.

2.5 Shear strength distribution of fins

In the calculation of the shear yield stress of the fins, the Saint-Venant principle is adopted. The distribution of shear stress and shear strength on the fin was influenced by the location and direction of the fin with respect to the strength vector (Doyle 1991, De Borst *et al*. 2012). In this study, the linearization is triangular and zero at the tip of the fins, following the principle of Saint-Venant. Conceptually, the investigation of shear stress distribution in fins analytically resembled the investigation of shear stress in the web, which was obtained using Eq. (1). The investigation of fin

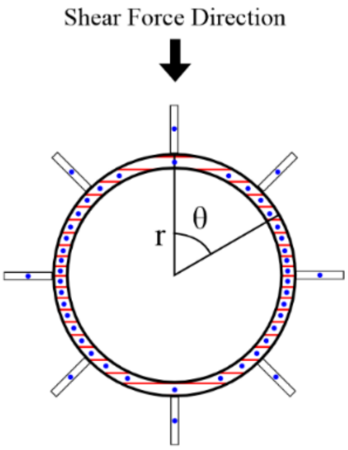

Fig. 8 Illustration of analytical segment division

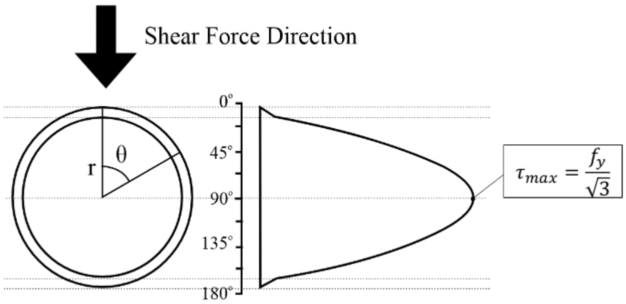

Fig. 9 Shear stress distribution of fins

shear stress must consider the angle of the fin direction. The direction of the fin shear stress vector must be parallel to that of the incident strength; they are summed up to contribute to the fin shear strength. Then, the shear stress that has been projected parallel to the strength vector can be integrated using Eq. (5) to obtain the fin shear strength.

2.6 Backbone curve parameters investigation

This study also observes structural behavior and performance by examining the backbone parameters. The backbone curve describes the resistance and energy dissipation stability of the MFCSHD during inelastic deformation under earthquake load. The backbone parameters include yield displacement (δ_y), maximum displacement (δ_{max}), shear yield strength (V_y), and maximum strength (V_{max}). These parameters can be used to determine the values of elastic stiffness (K_0), and post-yield stiffness (K_h), as illustrated in Fig. 10 (Sabouri-Ghomi *et al*. 2005, Hashimoto 2016). Those backbone curve parameters mentioned above are important for the seismic device design, i.e., V_y for the shear strength design, δ_y for the deformation state of the damper device starts to achieve energy dissipation, larger K_h indicates better inelastic shear resistance stability, and δ_{max} for the deformation capacity in remain stable shear resistance. The V_{max}/V_y ratios were also investigated to estimate the maximum shear strength in the design of MFCHSD. The positive trend of post-yield stiffness when the seismic device undergoes long inelastic deformation indicates that the device has good seismic performance.

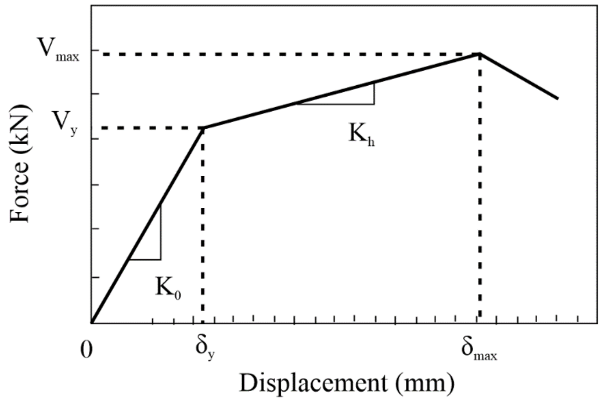

Fig. 10 Schematic backbone curve of MFCHSD

3. Result and discussion

3.1 Shear yield stress distribution

The shear yield stress analysis of the CHSD and MFCHSD Web demonstrated almost identical distribution results in the analytical and numerical calculations, confirming the concurrence of both methods, as shown in Fig. 11.

On the other hand, a difference in stress between the analytical and numerical approaches was observed at the edge of the web-fin connection boundary. A significant drop in shear stress was noted at this location. This discrepancy arose because the numerical approach was able to capture the effect of web stress transfer to the fins, which carried the load. The relative root mean square error (RRMSE) calculation of the stress results for the web at each 5º data interval between the analytical and numerical approaches, as shown in Table 1, indicated that most relative errors remain below 5%. Additionally, based on the comparison of the web's stress-area integration (Table 1) between the analytical and numerical results, most relative error was also found to be below 5%, except for the V4 PFL model. These findings indicate that the analytical results were a good agreement with the numerical results.

Under the yield state, the shear stress in the V0 specimen model was evenly distributed at an angle close to 90°. The shear yield stress was predominantly distributed along the half-diameter side of the tube in the direction of the 90° angle, as noted by Bukkems (2017). In general, for the V0 variation, the shear stress occurred mainly on the side of the 90° angle direction and decreased progressively in the 0° and 180° directions, as shown in Fig. 11(a). This phenomenon is attributed to the first moment of area (Q) of the CHS section, which gradually increases toward the center or deeper part of the section.

According to Fig. 11, in the general trend, the presence of fins affected sharper shear stress distribution that occurs on the deeper side web from the fins. In contrast, the web located at the outer side of the fins generated a flatter shear

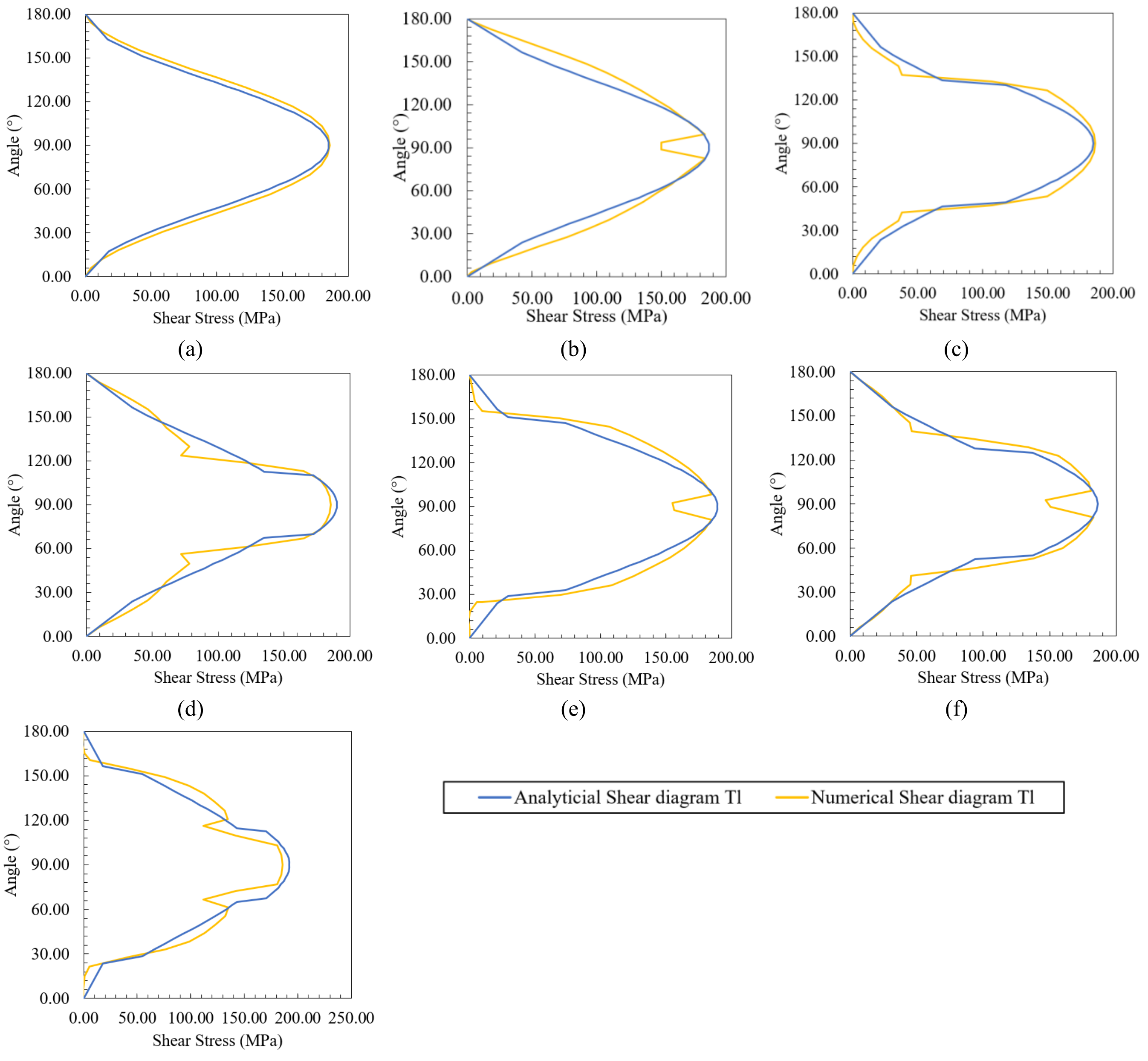

Fig. 11 Shear stress distribution of CHS web: (a) V0, (b) V4 PFL, (c) V4 CFL, (d) V6 PFL, (e) V6 CFL, (f) V8 PFL, and (g) V8 CFL

stress distribution. The reason is the appearance of fins increases the moment inertia in the general section and the first-moment area on the deeper side of the fins. However, it does not increase the first-moment area on the outer side of the fins.

The PFL and CFL directions of the V4 variation exhibited distinct behaviors. The shear stress distribution for the PFL V4 variation slightly widened with a gentle gradient, resembling the V0 variation. In contrast, the CFL V4 variation showed a sharper gradient in the angle range of 45° to 135°. As illustrated in Figs. 11(b)-11(c), the increase in shear yield stress sharpness for the V4 PFL variation occured across the entire 0° to 180° range, whereas for the V4 CFL variation, it occurred between 45° and 135°. Consequently, the shear coefficient for the V4 PFL variation is larger than that of the V4 CFL variation, as shown in Table 1.

According to Fig. 11, specimen V6 shows that CFL tends to have a greater area of shear yield stress than PFL. As illustrated in Figs. 11(d) and 11(e), the increase in shear yield stress for the V6 PFL variation occurs in the 60° to 120° angle range, while for the V6 CFL variation, it occurred between 30° and 150°. Consequently, the shear coefficient for the V6 CFL variation is greater than that of the V6 PFL variation, as presented in Table 1.

The V8 PFL and CFL exhibited comparable web shear stress distributions and shear stress areas, as shown in Figs. 11(f)-11(g). The graph in Fig. 11(f) indicated that for the V8 PFL variation, the sharp increase in shear yield stress occurred only after an angle of 45°. The V8 CFL variation

Table 1 Comparison of stress distribution characteristics of the web

Model Variables	RRMSE of Web's Stress Distribution Between Analytical and Numerical Results (%)	Relative Error of Web's Stress-Area Integration Between Analytical and Numerical Results (%)	Shear Coefficient of The Web (k)	
			Analytical	Numerical
V0	1.24	−1.32	0.51	0.54
V4 PFL	2.35	−10.10	0.53	0.59
V4 CFL	1.45	−2.33	0.45	0.48
V6 PFL	2.08	−0.09	0.47	0.48
V6 CFL	2.34	−5.05	0.48	0.56
V8 PFL	1.95	−2.78	0.48	0.51
V8 CFL	2.39	−0.79	0.49	0.49

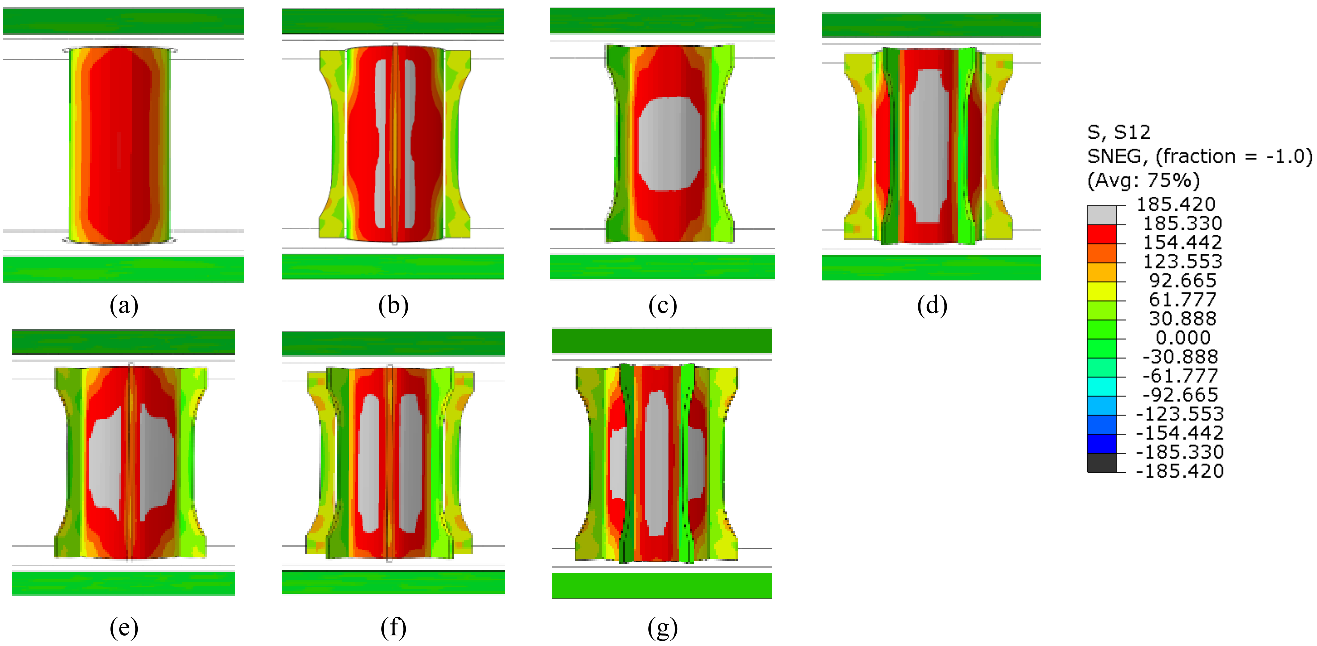

Fig. 12 Shear yield stress: (a) V0, (b) V4 PFL, (c) V4 CFL, (d) V6 PFL, (e) V6 CFL, (f) V8 PFL, and (g) V8 CFL

exhibited two distinct shear stress sharpens at 30° and 60°, with the general shape of the curve aligning with that of the V8 PFL. According to the shear stress area integration calculation, as presented in Table 1, the shear coefficients for both variations were relatively similar. Therefore, under probable multidirectional shear loading, the V8 specimen model demonstrated the best consistency in generating shear stress distribution and shear coefficient.

According to the shear stress and maximum principle stress contour check, as shown in Figs. 12-13, in the yield state, the yielding occurrence was dominated by shear stress in the web (grey color). While in the fins, the shear stress was below the yielding limit. Only the transition curve zone edge of fins occured the axial yielding stress. This finding suggests that the presence of fins does not result in a stress concentration effect in the web-fins connection boundary under the initial yielding state. Except, there was axial yielding stress of the transition curve zone edge of the fins. This phenomenon was also a coincidence with the study result by Utomo and Antonius (2018). The yielding area has potential tearing under large inelastic deformation due to over the stress limit. The aspects to be noted regarding the limitations of this modeling are the rigidity of the welded joint and the influence of residual welding stress on the connection between the tube and the fin, which have not yet been considered. The potential occurrence of additional stress concentration needs to be examined experimentally for future research.

3.2 Shear yield strength investigation

The shear yield strength of the CHSD V0 variation obtained through analytical and numerical methods showed good agreement results. The analytical result was 14.13 kN, while the numerical result was slightly higher at 14.32 kN, with difference of −1.33%. This discrepancy occurs because the numerical shear stress distribution for the V0 variation, as shown in Table 2, covers a slightly larger area than the analytical result. This finding aligns with the principle that shear yield strength is directly proportional to the shear stress distribution area. Additionally, the shear yield strength calculated using the American Institute of Steel Construction 360-16 (AISC 2016) formula in Eq. (4) yields a slightly larger value of 14.40 kN, differing by 1.91% from

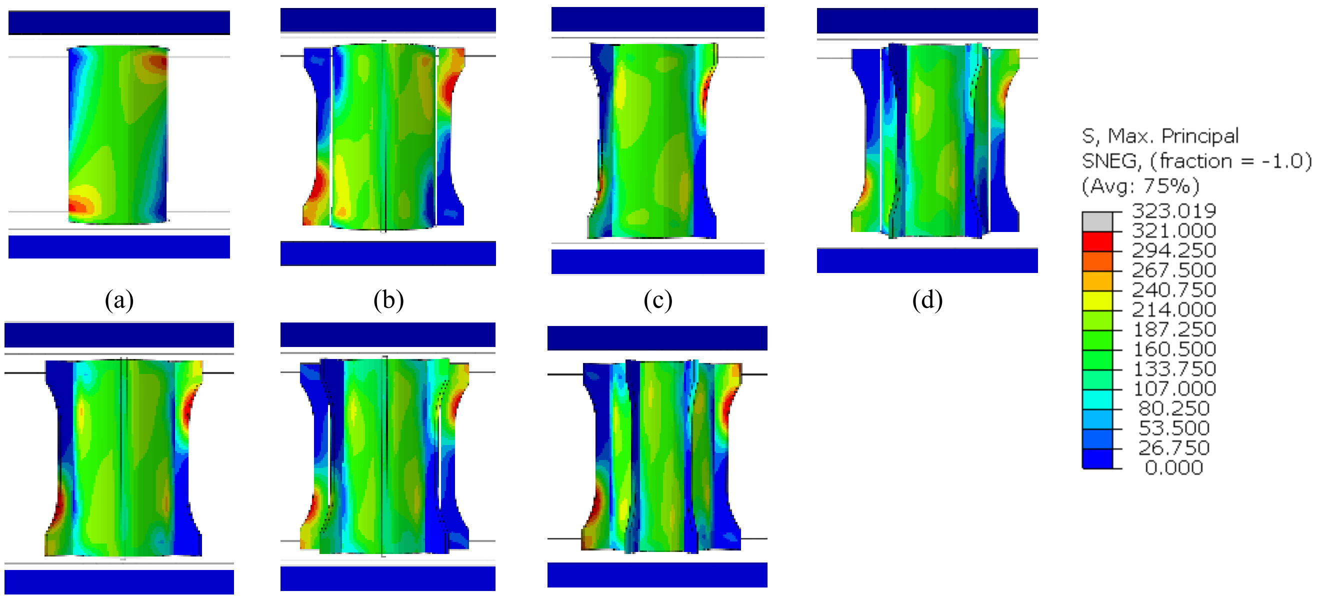

Fig. 13 Maximum principal stress: (a) V0, (b) V4 PFL, (c) V4 CFL, (d) V6 PFL, (e) V6 CFL, (f) V8 PFL, and (g) V8 CFL

Table 2 Shear yield strength comparison in slender CHSD and MFCHSD using analytical and numerical approaches

Variant	Analytical Shear Yield Strength (kN)			Numerical Shear Yield Strength (kN)	Relative Difference (%)
	Web	Fins	Total		
V0	14.13	-	14.13	14.32	−1.33
V4 PFL	14.67	2.86	17.53	17.61	−0.45
V4 CFL	13.19	2.93	16.11	15.51	3.87
V6 PFL	13.37	3.45	16.81	18.20	−7.64
V6 CFL	14.60	4.17	18.77	18.80	−0.16
V8 PFL	13.60	5.84	19.44	19.68	−1.22
V8 CFL	13.93	5.85	19.78	19.69	0.46

Table 3 Shear yield strength comparison in stocky CHSD and MFCHSD using analytical and numerical approaches

Variant	Analytical Shear Yield Strength (kN)			Numerical Shear Yield Strength (kN)	Relative Difference (%)
	Web	Fins	Total		
V0	42.29	-	42.29	42.44	−0.35
V4 PFL	45.45	9.32	54.77	56.54	−3.24
V4 CFL	38.27	11.42	49.70	49.30	0.80
V6 PFL	40.73	10.65	51.38	55.78	−8.56
V6 CFL	41.55	15.70	57.25	57.01	0.41
V8 PFL	42.30	18.95	61.24	60.16	1.77
V8 CFL	42.73	17.38	60.11	60.67	−0.92

the analytical approach. These results confirm the validity of shear yield strength calculations using both shear stress integration and the formula approach from AISC 360-16, demonstrating that the analytical method effectively represents the shear yield stress distribution in the V0 variation.

The MFCHSD variations V4 to V8 have an irregular CHS shape, which results in differences in stress distribution, as shown in Fig. 11, and variations in the shear coefficient, as presented in Table 1. Therefore, a developed calculation method is employed to determine the shear yield stress, which slightly differs from that of the V0 variation. In these variations, the fin shear strength must be considered and is calculated using Eq. (5). Additionally, the number of fins in variations V4 to V8 influences the total shear yield strength for each variation.

Based on the analytical calculations presented in Table2, an increase in the number of fins corresponds to a higher

Table 4 Comparison of the proposed analytical formulation and the numerical results of slender CHSD and MFCHSD

Variant	Shear Yield Strength (kN)		Relative Difference (%)
	Analytical	Numerical	
V0	14.40	14.32	−0.56
V4 PFL	17.60	17.61	0.06
V4 CFL	16.05	15.51	−3.36
V6 PFL	17.68	18.2	2.94
V6 CFL	18.75	18.8	0.27
V8 PFL	19.69	19.68	−0.05
V8 CFL	19.94	19.69	−1.25

Table 5 Comparison of the proposed analytical formulation and numerical results of stocky CHSD and MFCHSD

Variant	Shear Yield Strength (kN)		Relative Difference (%)
	Analytical	Numerical	
V0	42.29	42.44	0.35
V4 PFL	54.25	56.54	4.05
V4 CFL	49.58	49.3	−0.57
V6 PFL	54.77	55.78	1.81
V6 CFL	57.19	57.01	−0.32
V8 PFL	61.13	60.16	−1.61
V8 CFL	62.98	60.67	0.62

total shear yield strength. The use of four to eight fins enhances the shear yield strength within a range of 20% to 40% from the web shear yield strength. The direction of loading in PFL and CFL generates difference shear yield strength achievement in the same number of the fins. The relative differences were 2.39%, 17.27%, and 7.85% for V4, V6, and V8, respectively. However, the shear yield strength of CHS webs with fins does not exceed that of the regular CHS web (V0) except in the case of V4 PFL. Furthermore, it exhibits slight fluctuations depending on the shear coefficient, as shown in Table 1. Thus, the shear yield strength achievement with variations V4, V6, and V8 has increased pattern.

Based on the trend of increasing the number of fins, the results were getting better shear yield strength enhancement. However, increasing the number of fins would be a challenge in the fabrication process. Thus, according to this study, the determination of fins number was limited to eight.

The shear yield strength results for the stocky CHSD and MFCHSD models with a D/t ratio of 19.4 were determined to ensure the accuracy of the model integration calculation. The fin dimension of the stocky models is designed to be proportional to the CHS thickness of the slender models. Table 3 shows that the results of the analytical shear stress integration for the stocky model were close to the numerical shear yield strength results. The difference between the analytical and numerical results was relatively small, indicating that the integration results were appropriate. In addition, Table 3 presents that the fin strength contribution of stocky CHS was also as proportional as to the slender CHS.

3.3 Shear yield strength formulation

The difference in shear yield strength on the CHSD web was not the primary factor, but it still impacted the total shear yield strength of CHSD. To accurately calculate the shear yield strength of the finned variation of CHSD, the shear strength must be adjusted by adding a shear coefficient (k) according to Eq. (4). In this study, the shear coefficient value is presented in Table 1.

The results showed that the fin shear stress was influenced by two factors: the angle of the fin with respect to the shear strength and the number of fins. The CHSD yield strength formula in Eq. (4) assumes the shear stress to be the shear yield stress (τ_y). Consequently, Eq. (6) is proposed to determine the fin shear strength. The shear stress on the fin was found to be equivalent to the web shear stress at the tip of the fin, wherein the web shear stress was dependent on the angle. Hence, an angular coefficient represented by β is necessary to modify the shear stress input in the formula for fin shear strength.

The analysis result of the angle and shear stress relationship exhibited a difference in shear stress between the V0 and MFCHSD variations. Specifically, at 0°, the shear stress in the V0 variation was 0 MPa, whereas that in the MFCHSD variation could be calculated using Eq. (1) on the fin section. The shear stress of the fin at 0° was defined as τ_{f0} and divided by the shear yield stress (τ_y) to obtain the ratio between τ_{f0} and τ_y. This ratio served as a coefficient in the linear equation to ensure that the stress at 0° was not 0 MPa. The relationship between the angle and the web shear stress magnitude can be approximated using linear regression in Eq. (7) with a correlation value of 0.99. The variable x represents sin(θ), which is the angle input. The ratio between τ_{f0} and τ_y functions so that the β value is not zero when the angle input is 0°. Conceptually, the shear stress at each angle did not exceed the shear yield stress, allowing a maximum value of β at 1. Thus, the formula for m was crafted to be one minus the ratio of τ_{f0} to τ_y, divided by sin (90°), where 90° is the maximum angle. This linear function produces the coefficient of the ratio between shear stress at each angle and the shear yield stress, defined as the angle coefficient (β), as displayed in Eq. (8). Therefore, Eq. (9) demonstrates the methodology to determine the shear strength on one fin, where the value of τ_{f0} must include initial shear strength data (V_i). The iterative process became imperative to ascertain the shear strength using Eq. (9). This iterative calculation process can be facilitated by employing a solver program, thereby streamlining the procedure.

$$V_{yf} = \frac{\tau_y A_{fi}}{2} \tag{6}$$

$$y = m\,\mathrm{x} + c \tag{7}$$

$$\beta = \left(1 - \frac{\tau_{f0}}{\tau_y}\right)\sin(\theta) + \frac{\tau_{f0}}{\tau_y} \tag{8}$$

$$V_{yf} = \frac{\tau_y A_{fi} \beta}{2} \quad (9)$$

The shear strength of the MFCHSD was influenced by the web shear strength (V_{yw}) and fin shear strength (V_{yf}). The number of fins presented on the MFCHSD also affected the shear strength of the fin itself. The shear yield strength of the FCSHD was determined using Eq. (10). The values of the web coefficient (k) following the stress integration analysis as presented in Table 1. The analytical results of the shear strength of the slender MFCHSD were almost similar to the numerical ones, with a difference not exceeding 5%, as demonstrated in Table 4. This finding suggests that the following formula for determining the shear yield strength of MFCHSD is appropriate. The shear yield strength for the stocky CHSD and MFCHSD variants was calculated using Eq. (10). Table 5 shows that the results of the shear yield strength using Eq. (10) were close to the numerical results. This finding indicates that the proposed Eq. (10) for determining the shear yield strength is appropriate for both slender and stocky MFCHSD models.

$$V_y = \tau_y A_w k + \sum_{i=0}^{n} \frac{\tau_y A_{fi} \beta}{2} \quad (10)$$

3.4 Post-yield behavior

The loading results for the CHSD variations are presented in the backbone curve in Fig. 14. This graph indicates that the V0 variation had the lowest strength at 16.40 kN, among other variations. The V0 variation exhibited a decrease in stiffness after yielding due to the initial occurrence of inelastic web buckling that diminished its strength. Abebe *et al*. (2019) suggested that inelastic buckling occurred when the D/t ratio exceeded 27.8 in the V0 variation. The findings revealed that the V0 variation possessed the lowest maximum displacement capacity value and maximum strength of 16.40 kN.

Model variation V4 experienced buckling after exceeding the maximum displacement limit, indicating that adding four fins to the MFCHSD does not effectively stabilize the device. The addition of four fins to the V0 CHSD, with an effective fin length of 6.21 mm and a width of 2 mm, was intended to enhance web strength. However, the MFCHSD V4 variation exhibited a maximum strength of 21.86 kN in the PFL direction and 20.33 kN in the CFL direction. Despite the fin addition, variation V4 still showed strength degradation when the displacement exceeded 4 mm due to cyclic loading.

MFCHSD variations with the addition of six and eight fins produced better results than variations V0 and V4. Thus, six to eight fins on MFCHSD could improve strength and reduce strength degradation. Model variations V6 and V8 did not experience buckling at maximum displacement, suggesting higher stability. The graph in Fig. 14 shows that the maximum strength value of variation V6 in the PFL axis direction was 25.36 kN, whereas the CFL axis direction was24.26 kN. In addition, in the V6 variation, strength degradation only occurred when the displacement reached

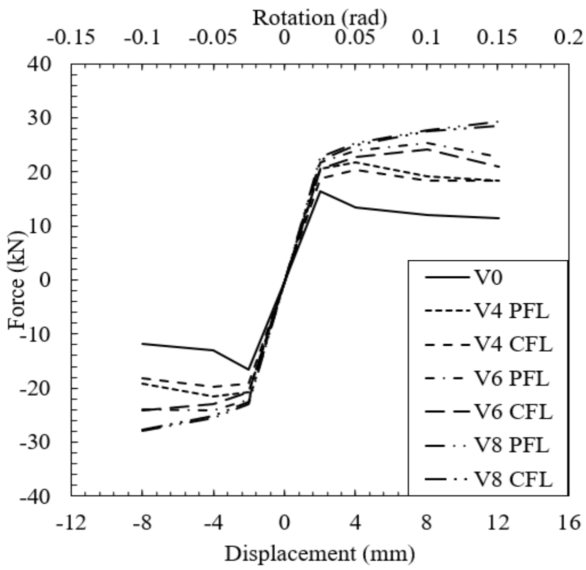

Fig. 14 Backbone curve of slender CHSD and MFCHSD variant

8.03 mm. For variation V8, the maximum strength achieved was 29.30 kN without strength degradation. Thus, V8 was the most stable variation in resisting cyclic loads. The analysis results suggest that the V8 variant had not experienced any strength degradation because the loading protocol was limited to 12.09 mm.

Increasing the number of fins in each MFCHSD variation typically leads to a higher maximum strength value. The results indicate a direct correlation between the number of fins and maximum strength: more fins lead to greater maximum strength value achieved by the MFCHSD. Furthermore, the results reveal that, in terms of maximum strength, the PFL variation always outperformed the CFL variation in V4 and V6. Specifically, variations V4 and V6 manifest that the maximum strength value for the PFL variation exceeded that of the CFL variation. The addition of fins has an impact on the greater strength and post-yield stiffness stability against buckling under inelastic lateral shear deformation as the given loading protocol. It needs to be noted that due to the earthquake scenario that may occur several times, there needs to be further study about the low cyclic fatigue effect on MFCHSD.

Based on the research of Abebe *et al*. (2019) states that CHSD will occur premature buckle when its D/t value exceeds 27.8. In the context of MFCHSD, the D/t value is represented by the unconfined chord length (L_c) to thickness (t) ratio of the tubular web, where the unconfined chord length is the calculated length between closer fins. The smaller value of L_c/t ratio indicates a more stable tubular web. According to Table 6, additional 6 and 8 fins reduce the value of L_c/t ratio to be less than 27.8, resulting in better premature buckle prevention indicated by post-yield stability achievement.

The maximum yield strength ratio for CHSD and MFCHSD variations ranged from 1.18 to 1.45, as shown in Table 6. PFL direction strength ratios for V0 and V4 are similar to those of V4 and V6 variations in the CFL

Table 6 Comparison of displacement capacity, shear strength, and stiffness results of the slender MFCHSD

Variant	L_c/t	Displacement (mm)		Shear strength (kN)		Maximum-to-yield strength ratio	Stiffness		Post-yield to elastic stiffness ratio
		Yielding	Maximum	Yielding	Maximum		Elastic stiffness (kN/mm)	Post-yield stiffness (kN/mm)	
V0	48.6	0.28	2.00	14.32	16.40	0.024	50.47	1.21	0.024
V4 PFL	34.3	0.29	4.00	18.03	21.86	0.018	58.33	1.03	0.018
V4 CFL	34.3	0.28	4.00	15.51	20.33	0.023	54.66	1.30	0.023
V6 PFL	24.3	0.30	8.03	18.20	25.36	0.013	72.10	0.93	0.013
V6 CFL	24.3	0.30	8.03	18.80	24.26	0.010	71.44	0.71	0.010
V8 PFL	18.6	0.32	12.09	19.68	29.30	0.011	76.99	0.82	0.011
V8 CFL	18.6	0.32	12.09	19.69	28.53	0.018	75.33	0.76	0.018

direction. Variation V6 in the PFL direction and variation V8 recorded the largest ratio of 1.4. The average ratio was 1.3, confirming consistent comparison between the maximum strength values of the CHSD and MFCHSD variations. This result adheres to the research findings, indicating that the maximum value was 1.2 times the yield value (Hashimoto 2016, Ali Awaludin *et al*. 2022).

According to Table 6, there are different behaviors found between elastic stiffness and post-yield stiffness. Elastic stiffness consistently increased as the number of fins in the device increased, whereas post-yield stiffness exhibited the opposite behavior. This phenomenon was due to the cyclic loading at the post-yield that occurred three times at each displacement. As a result, stiffness was reduced when the strength reached its maximum value.

4. Conclusions

This study investigated the performance of a proposed multidirectional finned circular hollow steel damper (MFCHSD), an enhanced version of the conventional slender circular hollow steel damper. Both analytical and numerical analyses were conducted, leading to the following conclusions:

• The analytical and numerical modeling derived from finite element analyses suggested that the proposed formula for estimating the shear yield strength of the MFCHSD is reasonably accurate and consistent. The relative differences in shear yield strength achievement between the analytical approach and numerical modeling were generally small, with most values below 5%.

• Additional fins number generated supplemental shear resistance supporting the CHS web, which in turn improved the overall shear yield strength of the device. Furthermore, both the number of fins and the loading direction (parallel and crossing to the fin axis) influenced the distribution of shear yield stress and affected the shear coefficient. Among the configurations tested, the MFCHSD with eight fins demonstrated the most consistent and highest shear yield strength across both loading directions.

• The post-yield behavior of the MFCHSD was also influenced by the number of fins, with a larger fin number (lower L_c/t value) resulting in prevented premature buckle and enhanced post-yield stiffness stability. Specifically, the V6 and V8 variations exhibited superior stability compared to V4, while the non-finned variant, V0, exhibited inferior stability. According to the results of the post-yield analysis of MFCHSD, the maximum-to-yield strength ratio ranged between 1.18 and 1.45. Then, the post-yield to elastic stiffness ratio value ranges from 0.010 to 0.024.

• According to the performance and mechanical behavior achievement, the proposed MFCHSD has the potential to be implemented as an additional seismic energy dissipation device for a new bridge structure or seismic performance retrofitting purpose of an existing bridge structure. However, constructive studies for the development of MFCHSD are still to be needed, i.e., fatigue failure mitigation due to service traffic load and experimental study to confirm the real achievement. The effect of the rigidity and residual stress of the welding connection between fins to the web also needs to be investigated through experimental study.

Acknowledgements

The authors are grateful to the Department of Civil and Environmental Engineering at Universitas Gadjah Mada for the software license support. The authors are grateful to the Badan Penerbit dan Publikasi Universitas Gadjah Mada for their invaluable assistance in editing this manuscript. The following authors contributed to this study: Ali Awaludin in writing, conceptualizing, reviewing, and editing; Andika Monanta Emildardi in data analyzing, writing, and editing; Angga Fajar Setiawan in conceptualizing, data analyzing, writing, reviewing, and editing; Iman Satyarno in reviewing and advicing.

References

Abebe, D.Y., Kim, J.W., Gwak, G. and Choi, J.H. (2019), "Low-cycled hysteresis characteristics of circular hollow steel damper subjected to inelastic behavior", *Int. J. Steel Struct.,* **19**(1), 157-167. https://doi.org/10.1007/s13296-018-0097-8.

AISC 310-16 (2016), *Specification for Structural Steel Buildings*, American Institute of Steel Construction; Chicago, Illions, USA.

Awaludin, A., Setiawan, A.F., Satyarno, I., Shuanglan, W. and Haroki, Y. (2022), "Finite element analysis of bi-directional shear panel damper with square hollow section under monotonic loading", *J. Civil Eng. Forum*, 157-168. https://doi.org/10.22146/jcef.3842.

Bukkems, J.M.W (2017), "Bending-shear interaction of circular hollow sections assessment of the cross-sectional design rules by means of analytical, numerical and statistical evaluation", www.tue.nl

Chaboche, J.L. (1986), "Time-independent constitutive theories for cyclic plasticity", *Int. J. Plasticity,* **2**(2), 149-188. https://doi.org/10.1016/0749-6419(86)90010-0.

Chaofeng, Z., Youchun, W., Longfei, W. and Meiping, W. (2017), "Hysteretic mechanical property of low-yield strength shear panel dampers in ultra-large plastic strain", *Eng. Struct.*, 11-22. https://doi.org/10.1016/j.engstruct.2017.06.028.

Chen, Z., Ge, H. and Usami, T. (2006), "Hysteretic model of stiffened shear panel dampers", *J. Struct. Eng.,* **132**(3), 478-483. https://doi.org/10.1061/(asce)07339445(2006)132:3(478).

Cowper, G.R. (1966), "The shear coefficient in timoshenko's beam theory", *J. Appl. Mech.,* **33**(2), 335-340. https://doi.org/10.1115/1.3625046.

De Borst, R., Crisfield, M.A., Remmers, J.J. and Verhoosel, C.V. (2012), *Non-Linear Finite Element Analysis of Solids and Structures Wiley Series in Computational Mechanics Series Advisors*, John Wiley and Sons, Chichester, United Kingdom.

Doyle, J.F. (1991), *Static and Dynamic Analysis of Structures with An Emphasis on Mechanics and Computer Matrix Methods*. West Lafayette: Aeronautics and Astronautics Department. Purdue University

Emilidardi, A.M., Fajar, A.S., Awaludin, A., Satyarno, I. and Sunarso, M. (2022), "Numerical model of finned tubular shear panel damper for multi-direction seismic excitation", In *Proceedings of the 5th International Conference on Sustainable Civil Engineering Structures and Construction Materials*, 751-66. Singapore, Springer. https://doi.org/Https://doi.org/10.1007/978-981-16-7924-7_49.

Feng, R., Huang, Z., Chen, Z., Roy, K., Chen, B. and Lim, J.B. (2021a), "Experimental study on material properties and stress concentration factors of stainless-steel hybrid tubular joints", *Construct. Build. Mater.,* **267**(January). https://doi.org/10.1016/j.conbuildmat.2020.121103.

Feng, R., Wu, C., Chen, Z., Roy, K., Chen, B. and Lim, J.B. (2021b), "Finite element modelling and proposed design rules of stainless steel hybrid tubular joints with square braces and circular chord", *J. Construct. Steel Res.,* **179**(April). https://doi.org/10.1016/j.jcsr.2021.106557.

Feng, R., Xu, J., Chen, Z., Roy, K., Chen, B. and Lim, J.B. (2021c), "Numerical investigation and design rules for stress concentration factors of stainless-steel hybrid tubular joints", *Thin-Wall. Struct.,* **163**(June). https://doi.org/10.1016/j.tws.2021.107783.

Ghosh, K., Roy, K., Tiwari, S., Fang, Z., Paul, B. and Lim, J.B. (2025), "Axial capacity of cold-formed steel channel sections with slits", *Eng. Struct.,* **322**(January). https://doi.org/10.1016/j.engstruct.2024.119094.

Guo, W., Ma, C., Yu, Y., Bu, D. and Zeng, C. (2020), "Performance and optimum design of replaceable steel strips in an innovative metallic damper", *Eng. Struct.,* **205**(December 2019), 110-118. https://doi.org/10.1016/j.engstruct.2019.110118.

Han, Q., Zhou, Y., Ou, Y. and Du, X. (2017), "Seismic behavior of reinforced concrete sacrificial exterior shear keys of highway bridges", *Eng. Struct.,* **139**, 59-70. https://doi.org/10.1016/j.engstruct.2017.02.034.

Hashimoto, K. (2016), "Effect of structural parameters of shear panel damper on seismic performance of multi-pipe integrated bridge pier", *J. JSCE,* **72**(1), 75-91.

Hutchinson, J.R. (2001), "Shear coefficients for timoshenko beam theory", *J. Appl. Mech. Transact., ASME,* **68**(1), 87-92. https://doi.org/10.1115/1.1349417.

Javanmardi, A., Ibrahim, Z., Ghaedi, K., Benisi Ghadim, H. and Hanif, M.U. (2020), "State-of-the-art review of metallic dampers: testing, development and implementation", *Archiv. Comput. Meth. Eng.,* **27**(2), 455-478. https://doi.org/10.1007/s11831-019-09329-9.

Li, H., Jiang, K., Chen, Y. and Han, X. (2019), "Multi-directional energy dissipation anti-buckling metal pipe damper", CN110284615A.

Men, J., Wang, J., Zhang, Q., Fan, D., Zhou, Q. and Huang, C.H. (2023), "Experimental and numerical study on cyclic behavior of a shape-optimized composite metallic yield damper with two-phase energy dissipation", *Structures,* **53**(July), 1012-1029. https://doi.org/10.1016/j.istruc.2023.05.007.

Nuzzo, I., Losanno, D., Caterino, N., Serino, G. and Rotondo, L. M.B. (2018), "Experimental and analytical characterization of steel shear links for seismic energy dissipation", *Eng. Struct.,* **172**(July 2017), 405-418. https://doi.org/10.1016/j.engstruct.2018.06.005.

Nyabongo, E. and Li, X (2024), "Development of energy-early-dissipated braces based on web buckling of low-yield i-section steel", *J. Construct. Steel Res.,* **217**(108672), 1-16. https://doi.org/10.1016/j.jcsr.2024.108672.

Omrani, R., Mobasher, B., Liang, X., Gunay, S., Mosalam, K.M., Zareian, F. and Taciroglu, E. (2015), "Guidelines for nonlinear seismic analysis of ordinary bridges: version 20", *Ca15-2266*, **168**. https://doi.org/10.13140/rg.2.1.4946.6648.

Sabouri-Ghomi, S., Ventura, C.E. and Kharrazi, M.H. (2005), "Shear analysis and design of ductile steel plate walls", *J. Struct. Eng.,* **131**(6), 878-889. https://doi.org/10.1061/(asce)0733-9445(2005)131:6(878).

Setiawan, A.F., Takahashi, Y., Kiyono, J. and Sawada, S. (2017), "Numerical analysis of rc columns accompanied with friction damping mechanism under cyclic loading", In *Procedia Eng.*, **171**(2017), 821-835, https://doi.org/10.1016/j.proeng.2017.01.373.

Tanaka, K. and Sasaki, Y. (2000), "Hysteretic performance of shear panel dampers of ultra low- yield-strength steel for seismic response control of buildings", 12th WCEE, **1248**, 1-8.

Timoshenko, S.P. (1921), "On the correction for shear of the differential equation for transverse vibrations of prismatic bars", *London, Edinburgh, Dublin Philosophic. Mag. J. Sci.,* **41**(245), 744-746. https://doi.org/Https://doi.org/10.1080/14786442108636264.

Utomo, J. (2018) "Improving resilience of moment frames using steel pipe dampers", *MATEC Web Conferences,* **195**, 1-8. https://doi.org/10.1051/matecconf/201819502014.

Utomo, J., Moestopo, M., Surahman, A. and Kusumastuti, D. (2015), "Estimating the ultimate energy dissipation capacity of steel pipe dampers", *Procedia Eng.,* **125**, 1101-1107. https://doi.org/10.1016/j.proeng.2015.11.128.

Vargas, R. and Bruneau, M. (2007), "Effect of supplemental viscous damping on the seismic response of structural systems with metallic dampers", *J. Struct. Eng.,* **133**(10), 1434-1444. https://doi.org/10.1061/(asce)0733-9445(2007)133:10(1434).

Varzaneh, M.N. and Hosseini, M. (2019), "Cyclic performance and mechanical characteristics of the oval-shaped damper", *KSCE J. Civil Eng.,* **23**(11), 4747-4757. https://doi.org/10.1007/s12205-019-1382-6.

Wang, W., Roy, K., Lu, L., Fang, Z. and Lim, J.B. (2024), "Simplified direct strength method for the design of cold-formed steel channels with circular web openings under two-flange loadings", *Eng. Struct.,* **319**(November). https://doi.org/10.1016/j.engstruct.2024.118840.

Wang, W., Roy, K., Rezaeian, H., Fang, Z. and Lim, J.B. (2025), "Moment capacity of cold-formed steel trusses with howick rivet connectors: tests, modelling and design", *Eng. Struct.,* **322**(2025), 119171, 1-16. https://doi.org/10.1016/j.engstruct.2024.119171.

Wang, W., Song, J., Wang, W., Ding, X. and Lu, Z. (2021), "Experimental investigation of the seismic behavior of low-yield-point corrugated steel plate dampers", *J. Struct. Eng.,* **147**(2), 04020335, 1-14. https://doi.org/10.1061/(asce)st.1943-541x.0002924.

Yang, J., Liang, S., Zhu, X., Dang, L., Shen, T. and Zhou, S. (2023), "Experimental and theoretical research on a shear-bending-metallic-damper with a double-phased yield mechanism", *J. Construct. Steel Res.,* **203**(2023) 107839, 1-20. https://doi.org/10.1016/j.jcsr.2023.107839.

Zhang, C., Aoki, T., Zhang, Q. and Wu, M. (2015), "The performance of low-yield-strength steel shear-panel damper with without buckling", *Mater. Struct. Materiaux et Construct.,* **48**(4), 1233-1242. https://doi.org/10.1617/s11527-013-0228-9.

Zhang, C., Zhang, Z. and Zhang, Q. (2012), "Static and dynamic cyclic performance of a low-yield-strength steel shear panel damper", *J. Construct. Steel Res.,* **79**, 195-203. https://doi.org/10.1016/j.jcsr.2012.07.030.

CC